nature climate change

LETTERS

PUBLISHED ONLINE: 16 MAY 2016 | DOI: 10.1038/NCLIMATE3029

Land–atmosphere feedbacks amplify aridity increase over land under global warming

Alexis Berg[1]*, Kirsten Findell[2], Benjamin Lintner[3], Alessandra Giannini[1], Sonia I. Seneviratne[4], Bart van den Hurk[5], Ruth Lorenz[6], Andy Pitman[6], Stefan Hagemann[7], Arndt Meier[8], Frédérique Cheruy[9], Agnès Ducharne[10], Sergey Malyshev[11] and P. C. D. Milly[12]

The response of the terrestrial water cycle to global warming is central to issues including water resources, agriculture and ecosystem health. Recent studies[1-6] indicate that aridity, defined in terms of atmospheric supply (precipitation, P) and demand (potential evapotranspiration, E_p) of water at the land surface, will increase globally in a warmer world. Recently proposed mechanisms for this response emphasize the driving role of oceanic warming and associated atmospheric processes[4,5]. Here we show that the aridity response is substantially amplified by land–atmosphere feedbacks associated with the land surface's response to climate and CO_2 change. Using simulations from the Global Land Atmosphere Coupling Experiment (GLACE)-CMIP5 experiment[7-9], we show that global aridity is enhanced by the feedbacks of projected soil moisture decrease on land surface temperature, relative humidity and precipitation. The physiological impact of increasing atmospheric CO_2 on vegetation exerts a qualitatively similar control on aridity. We reconcile these findings with previously proposed mechanisms[5] by showing that the moist enthalpy change over land is unaffected by the land hydrological response. Thus, although oceanic warming constrains the combined moisture and temperature changes over land, land hydrology modulates the partitioning of this enthalpy increase towards increased aridity.

Changes in water availability over land are a key driver of climate change impacts on human and natural systems. Observations[2] and model projections[1,3–6] point to the Aridity Index ($AI = P/E_p$, with annual-mean values) decreasing on average over land, corresponding to increasing aridity. This reflects the increase in global land evaporative demand from global warming[10] outpacing the precipitation increase[4,11]. Increasing aridity under climate change has recently been interpreted[4] in terms of the greater fractional change in E_p over land compared to the ocean. This results from enhanced near-surface warming over land[12–15] combined with declining relative humidity (RH), compared to a small RH increase over oceans[16–18]. Although land–ocean differences in moisture availability and surface energy budget have been invoked to explain such contrasts[13], a growing literature[5,14,15,18–20] emphasizes the role of ocean warming and atmospheric processes. In this view, the greater land-to-ocean warming is explained, at least in the tropics, in light of the zonal homogeneity of warming in the troposphere, combined with a smaller decrease in tropospheric lapse rate with warming over land, which is closer to dry adiabatic, than over oceans[14,15,19]. This land–ocean warming contrast is further invoked to explain the decrease of surface RH over land, with the argument that air masses advected from oceans contain insufficient water vapour to keep pace with the greater increase in saturation vapour pressure over land[5,15,18,20,21]. On the basis of such studies it has been argued[4,5] that the overall aridity increase over land is mainly driven by ocean–atmosphere processes. In particular, these studies imply that land surface processes, although possibly contributing, are unnecessary to explain increased aridity over land.

Nevertheless, key land surface processes potentially influence aridity changes. These include feedbacks from climate-change-induced long-term soil moisture changes on surface climate[7–9], and the physiological response of vegetation to increased atmospheric CO_2[22]. Here we assess the role of these processes on aridity projections. We make use of simulations from the multi-model GLACE-CMIP5 experiment[7], in which several modelling groups performed transient climate change simulations with (simulation SM_TRND) and without (SM_FIX) long-term trends in soil moisture (Methods). Another set of simulations includes runs with (CTL) and without (NoFERT) long-term changes in atmospheric CO_2 seen by vegetation, that is, the physiological effect of CO_2 (Methods). For each model, the same sea surface temperatures (SSTs) and radiative forcing agents (based on historical and RCP8.5 coupled simulations) were prescribed in all runs. Thus, comparing simulations SM_FIX and SM_TRND isolates the feedback on climate from long-term soil moisture changes; comparing CTL and NoFERT isolates the feedback from the vegetation response to increasing CO_2.

Projections of future soil moisture content by climate models generally exhibit negative trends[23] (Fig. 1 and Supplementary Fig. 1), consistent with overall land surface drying under global

[1]International Research Institute for Climate and Society, Columbia University, 61 Route 9W, Palisades, New York 10964-8000, USA. [2]Geophysical Fluid Dynamics Laboratory, 201 Forrestal Road, Princeton, New Jersey 08540, USA. [3]Department of Environmental Sciences, Rutgers, The State University of New Jersey, 14 College Farm Road, New Brunswick, New Jersey 08901, USA. [4]The Institute for Atmospheric and Climate Science, ETH Zürich, 8057 Zürich, Switzerland. [5]Royal Netherlands Meteorological Institute (KNMI), Utrechtseweg 297, 3731 GA De Bilt, The Netherlands. [6]ARC Center of Excellence for Climate System Science and Climate Change Research Center, University of New South Wales, New South Wales 2052, Australia. [7]Max Planck Institute for Meteorology, Bundesstraße. 53, D-20146 Hamburg, Germany. [8]Centre for Environmental and Climate Research, Sölvegatan 37, 223 62 Lund, Sweden. [9]Laboratoire de Météorologie Dynamique, Institut Pierre Simon Laplace, 4 place Jussieu, 75005 Paris, France. [10]UMR 7619 METIS, Institut Pierre Simon Laplace, 4 place Jussieu, 75005 Paris, France. [11]Princeton University & Geophysical Fluid Dynamics Laboratory Cooperative Institute for Climate Studies, Princeton, New Jersey 08540, USA. [12]US Geological Survey and NOAA/Geophysical Fluid Dynamics Laboratory Princeton, New Jersey 08540, USA. *e-mail: alexis.berg@noaa.gov

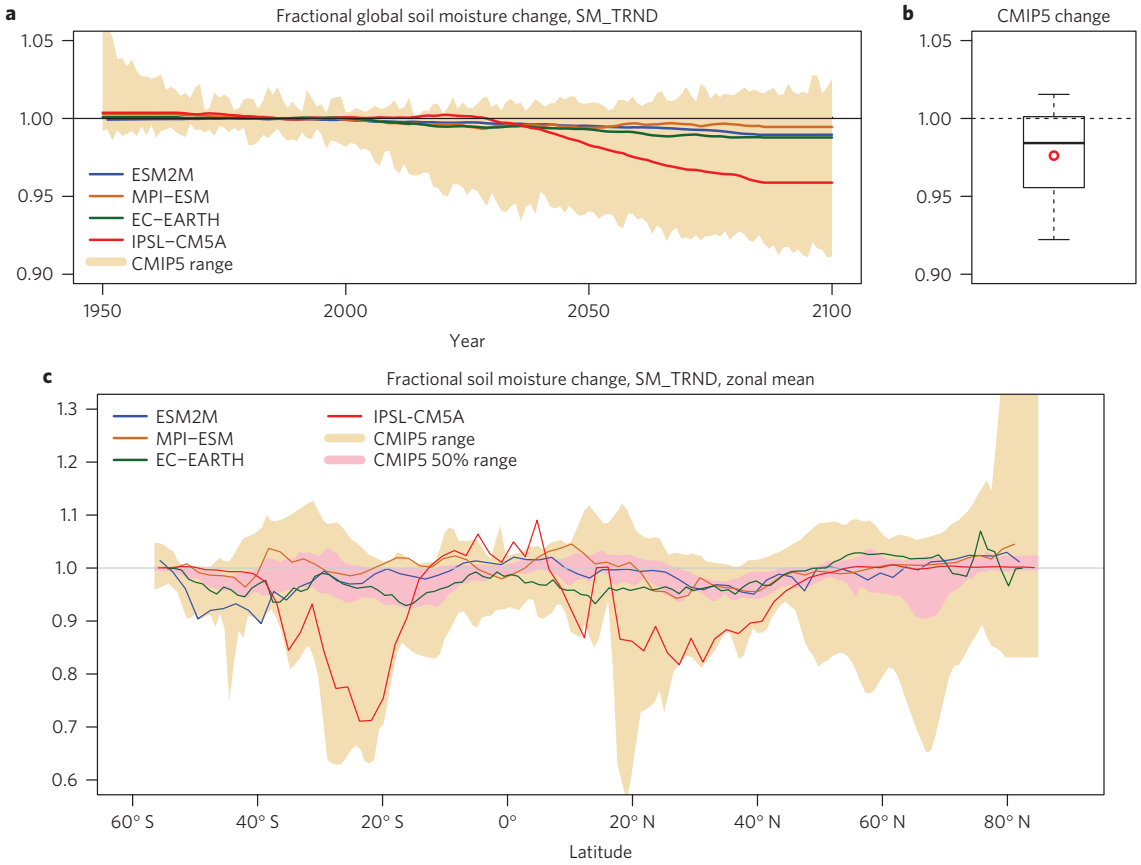

Figure 1 | Prescribed soil moisture trends. a, Trends in global, annual-mean, and total-column soil moisture, as a fraction of the average 1971–2000 global-mean value, in SM_TRND. Shading indicates the range of changes in an ensemble of 28 CMIP5 models, using historical and RCP8.5 simulations. See Supplementary Fig. 1 for individual models. **b**, Distribution of end-of-century fractional changes from the CMIP5 ensemble (whiskers indicate the total range, box edges indicate the first and third quartiles, middle bar indicates the median and red dot indicates the mean). **c**, Zonal fractional change in annual-mean soil moisture in simulation SM_TRND between 1971–2000 and 2071–2100. Shadings indicate the range of changes in the ensemble of 28 CMIP5 models.

warming. The four GLACE-CMIP5 models analysed here exhibit this behaviour (Fig. 1). Caution in interpreting trend differences is warranted because soil moisture is highly dependent on the model[24]: absolute soil moisture can vary substantially across models, and relative changes (Fig. 1) of similar magnitude may not imply similar impacts on surface fluxes. The global-mean negative trends mask spatial variability (Supplementary Fig. 2), consistent with large model spread in projected changes in land water balance[25]. Still, some agreement is evident for zonal-mean changes, with smaller decreases near the Equator and in high latitudes of the Northern Hemisphere, and larger decreases in the subtropics and mid-latitudes.

Figure 2 depicts the projected changes in global (land-only) annual-average surface climate in simulations SM_FIX and SM_TRND. In all models, the decreasing soil moisture trend in SM_TRND (Fig. 1) reduces the increase in terrestrial latent heat flux evident in SM_FIX. In terms of surface energy balance, this reduction is largely compensated by enhanced sensible heat flux and upwelling longwave radiation (not shown), both of which are associated with elevated skin temperature, and thus 2 m temperature (T), in SM_TRND. SM_TRND also manifests a greater reduction in continental cloud cover and thus greater surface incoming solar radiation, which amplifies the warming over land. With greater surface warming and reduction in specific humidity (Q), the projected decrease in RH over land is substantially enhanced in SM_TRND (∼−2.7%) compared to SM_FIX (∼−1%). The greater surface warming and larger relative humidity decrease in SM_TRND yield a greater increase in evaporative demand, as captured by Penman potential evapotranspiration E_p (Methods). By itself, the greater increase in E_p in SM_TRND enhances aridity (that is, lowers AI). However, the negative trends in soil moisture also have a positive feedback on precipitation, reducing the warming-induced increase in land precipitation (Fig. 2). For these reasons, AI decreases more strongly in SM_TRND than SM_FIX, highlighting the contribution of soil moisture changes to increasing continental aridity. Decomposing the fractional change of AI in each simulation into P- and E_p-related terms (Methods) indicates global contributions of 46% and 54%, respectively, to the enhanced aridity increase in SM_TRND.

Although the impacts of soil moisture changes on land climate are significant globally, they exhibit pronounced spatial heterogeneity (Supplementary Fig. 3, which illustrates this for evaporative demand). This heterogeneity mirrors regional soil moisture trends. For example, in all models, the greater increase in E_p in SM_TRND occurs primarily in regions with both low present-day soil moisture and projected soil moisture decreases (Fig. 3a). The impact of soil moisture changes on ΔE_p also results in distinct behaviours across latitudes (Fig. 3b): E_p enhancement is smallest around the Equator and largest in the subtropics and mid-latitudes. In MPI-ESM and IPSL-CM5A, this increase extends into (northern) high latitudes. Zonal patterns for ΔE_p reflect similar patterns for T, Q and RH (Supplementary Fig. 5). Because zonal changes in precipitation are more heterogeneous across the models than those of E_p (Supplementary Fig. 5), and because of the nonlinearity of AI

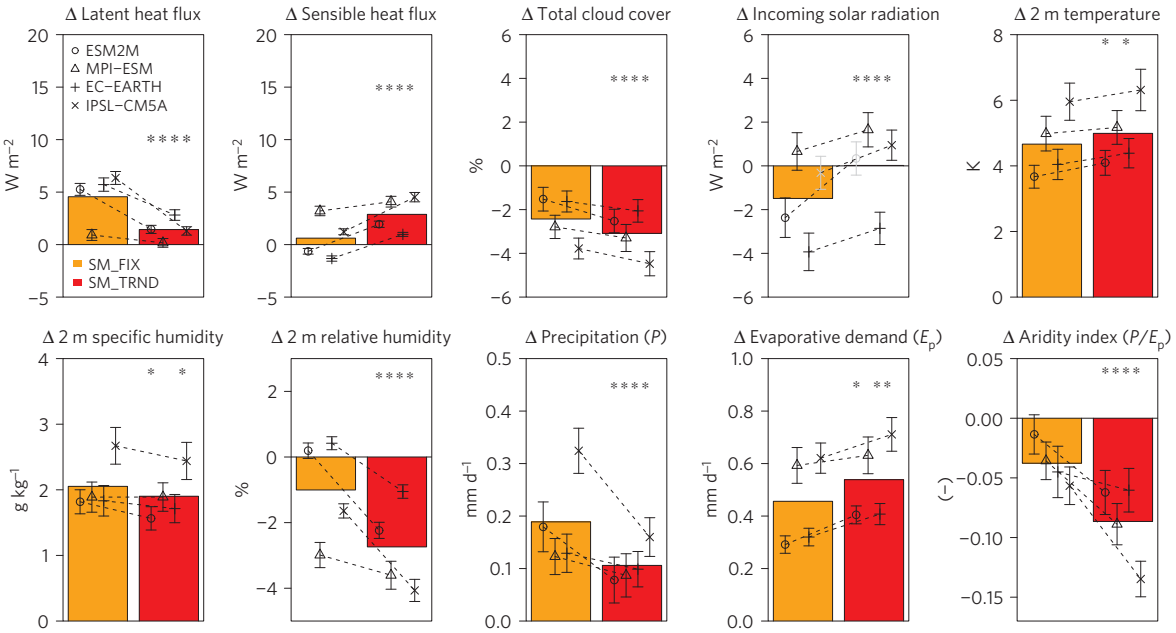

Figure 2 | Impact of soil moisture trends on land climate change. Bars represent multi-model mean changes in global (land-only), annual-mean surface climate in SM_FIX (orange) and SM_TRND (red) between the present (1971–2000) and future (2071–2100) (Δ = future minus present). Symbols represent individual models. Whiskers around symbols represent ±1 s.d. of annual means of the corresponding variable, estimated as pooled standard deviation over the present and future. Future-minus-present changes non-significantly different from zero are identified in grey. Asterisks over the SM_TRND bar indicate models for which the differences in future-minus-present change between SM_FIX and SM_TRND are statistically significant.

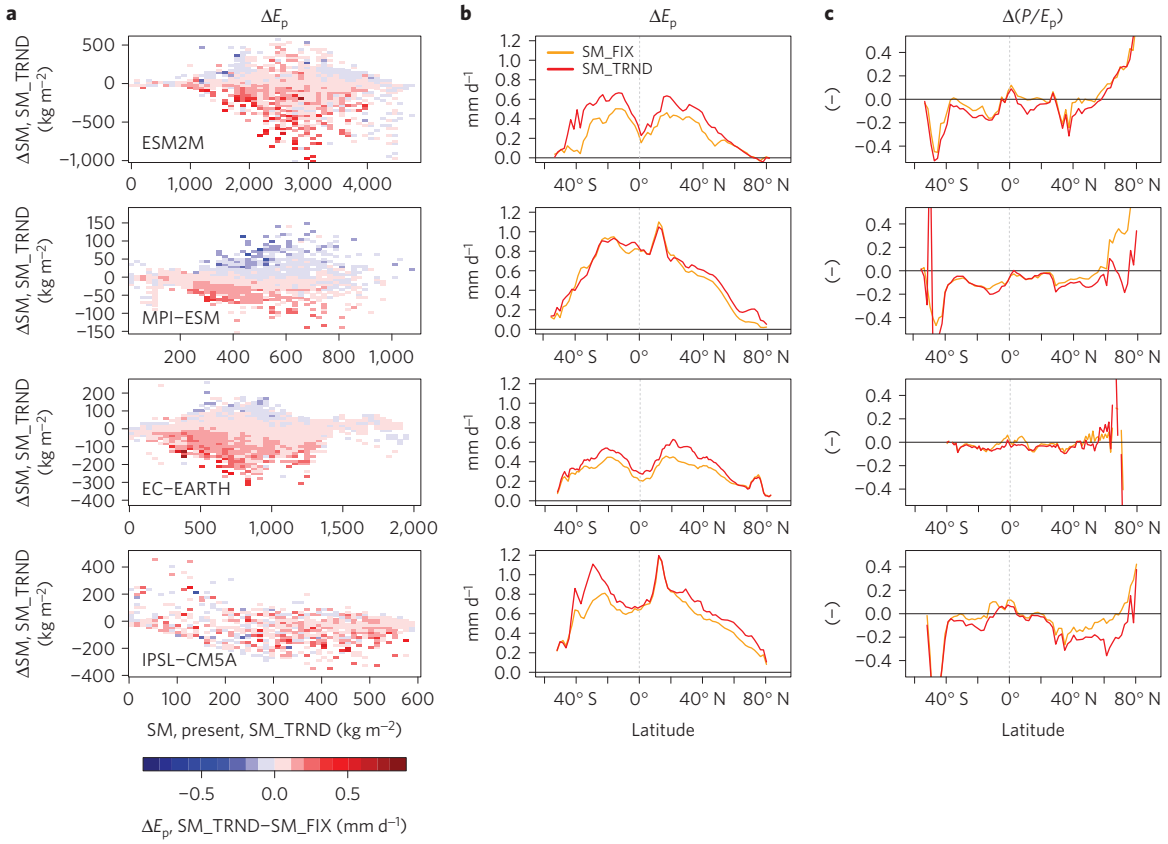

Figure 3 | Spatial variability of soil moisture impacts on aridity changes. a, SM_ TRND–SM_FIX difference in ΔE_p (Δ = future minus present) over land binned as a function of mean soil moisture (SM) in SM_TRND in the present (*x* axis) and future-minus-present soil moisture changes in SM_TRND (*y* axis). The density of these binned plots is shown on Supplementary Fig. 4—note that for IPSL-CM5A, most land pixels have mean soil moisture close to the model maximum of 600 kg m^{-2}, so that greater E_p increase in SM_TRND still occurs in pixels that are drier than the (model) average. **b**, Zonal ΔE_p in SM_FIX and SM_TRND (rows are models as in **a**). **c**, Same as **b**, but for the Aridity Index.

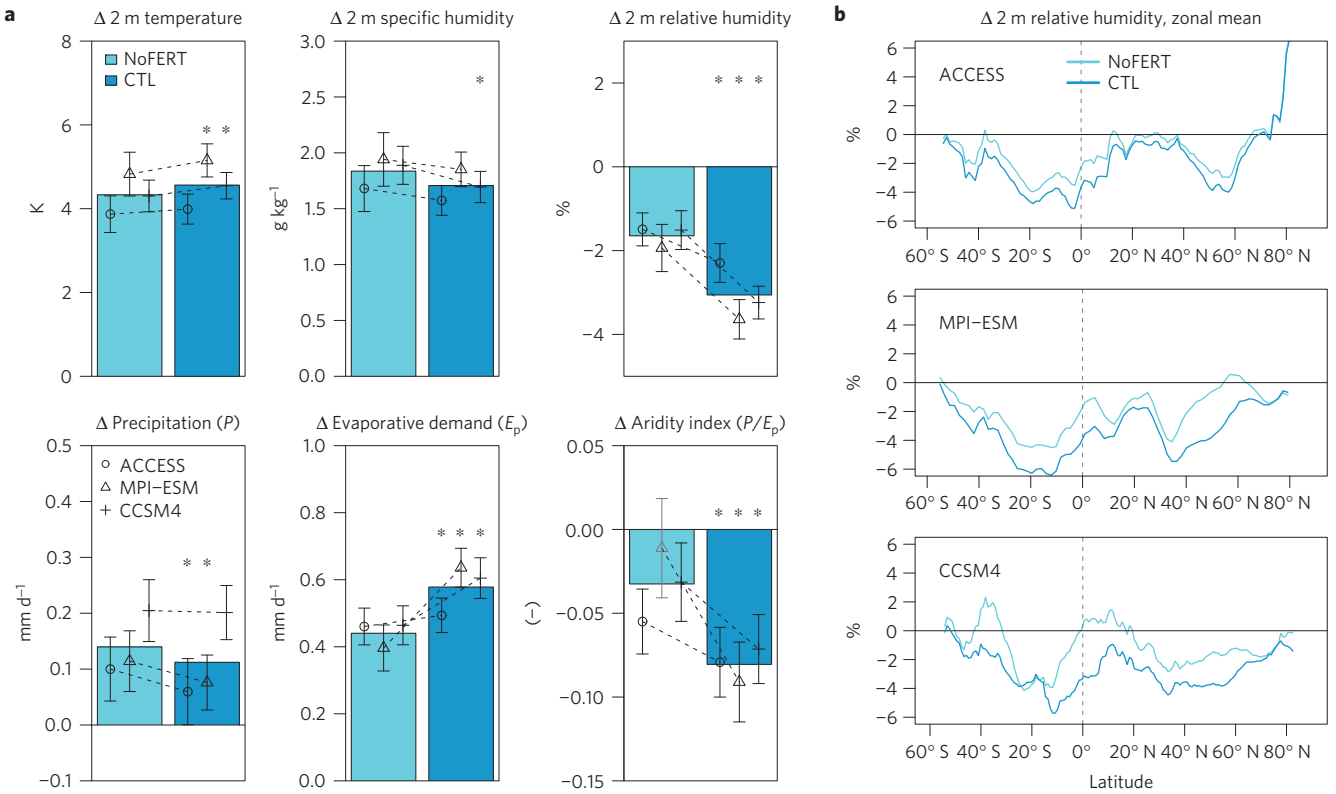

Figure 4 | Impact of CO_2 physiological effect on land climate change. a, Same as Fig. 2 for simulations NoFERT and CTL. Present-day for the ACCESS model is defined as 2007–2036 instead of 1971–2000 (Methods). For CCSM4, E_p was computed with a mean surface wind speed value (Methods) because of missing model outputs. **b**, Zonal change (future minus present) in surface relative humidity over land in NoFERT and CTL.

with respect to E_p, differences in $\Delta(P/E_p)$ exhibit more complex zonal patterns overall than ΔE_p (Fig. 3c), with some models yielding stronger enhancement in the middle and high latitudes, and others in the subtropics.

Similar results to those above are found in the simulations with and without the physiological effect of CO_2 in the twenty-first century. In these simulations, differences in near-surface climate are caused by stomatal closure in response to increased atmospheric CO_2 (ref. 22). With increased CO_2 in CTL, plant transpiration is reduced compared to NoFERT. The chain of processes leading to enhanced aridity in CTL compared to NoFERT is qualitatively similar to the soil moisture experiments (Fig. 4): increased land warming and drying enhancing evaporative demand, and reduced precipitation increase. The zonal patterns associated with these changes differ, however, with generally larger effects near the Equator, as is evident for the decrease in RH (Fig. 4b). This reflects the more uniform impact of CO_2 on vegetation compared to the regional soil moisture trends. Note that two of the models analysed (MPI-ESM and CCSM4) have an interactive leaf area index (LAI), and both simulate an increased global LAI from the CO_2 fertilization effect in CTL. Any enhanced evapotranspiration associated with increasing LAI is thus more than compensated by reduced evapotranspiration from stomatal closure in these models.

Although all models analysed agree on the signs of the effects investigated, inter-model spread exists in their magnitudes (Figs 2 and 4). This reflects model differences in projected changes in soil moisture (Fig. 1) or in representation of the physiological impacts of CO_2, but also in the strength of the simulated land–atmosphere coupling, in particular the feedback on precipitation[7–9,26]. Despite the qualitative robustness of these effects across models, the limited size of the model ensemble warrants caution when inferring their importance in other climate models. Another caveat involves the use of prescribed SSTs, which ignores possible feedbacks of ocean dynamics on land surface effects. The impact of such feedbacks is uncertain, but has generally been shown to slightly amplify the impacts of land perturbations such as deforestation[27]; our results are therefore likely to be conservative.

Different approaches have been used to compute E_p changes with climate change[1,3,4,10,28,29]. We obtain similar results to Fig. 2 when computing E_p as Penman–Monteith evapotranspiration[3,10] (Methods). Using simpler, net-radiation-based estimates (either directly as net radiation[29], or with the Priestley–Taylor formulation), E_p remains unchanged or is even reduced in SM_TRND compared to SM_FIX, reflecting the slight relative decrease in net surface radiation in SM_TRND, as greater surface warming is associated with increased upwelling longwave radiation. However, in this case, reduction in precipitation still leads to increased aridity (Supplementary Fig. 6). This highlights the key role of the positive feedback of decreasing soil moisture on precipitation. Our results are thus qualitatively robust to the approach used for calculating evaporative demand.

Overall, our analysis underscores a large contribution of land surface processes to increased continental aridity in response to global warming. Aridity does increase in experiments without soil moisture trends or the physiological effect of CO_2, in agreement with the proposed remote influence of ocean warming on land aridity changes[5]; however, this increase is substantially amplified by land–atmosphere feedbacks. In addition, we note that the 'without' simulation in each case still includes either the CO_2 effect (SM_FIX) or soil moisture changes (NoFERT), so that some of the aridity increase in these runs remains attributable to land surface effects. We also point out that although enhanced plant water use efficiency with increased atmospheric CO_2 may lead to lower AI values, this does not imply increased vegetation water stress. Rather, it stems

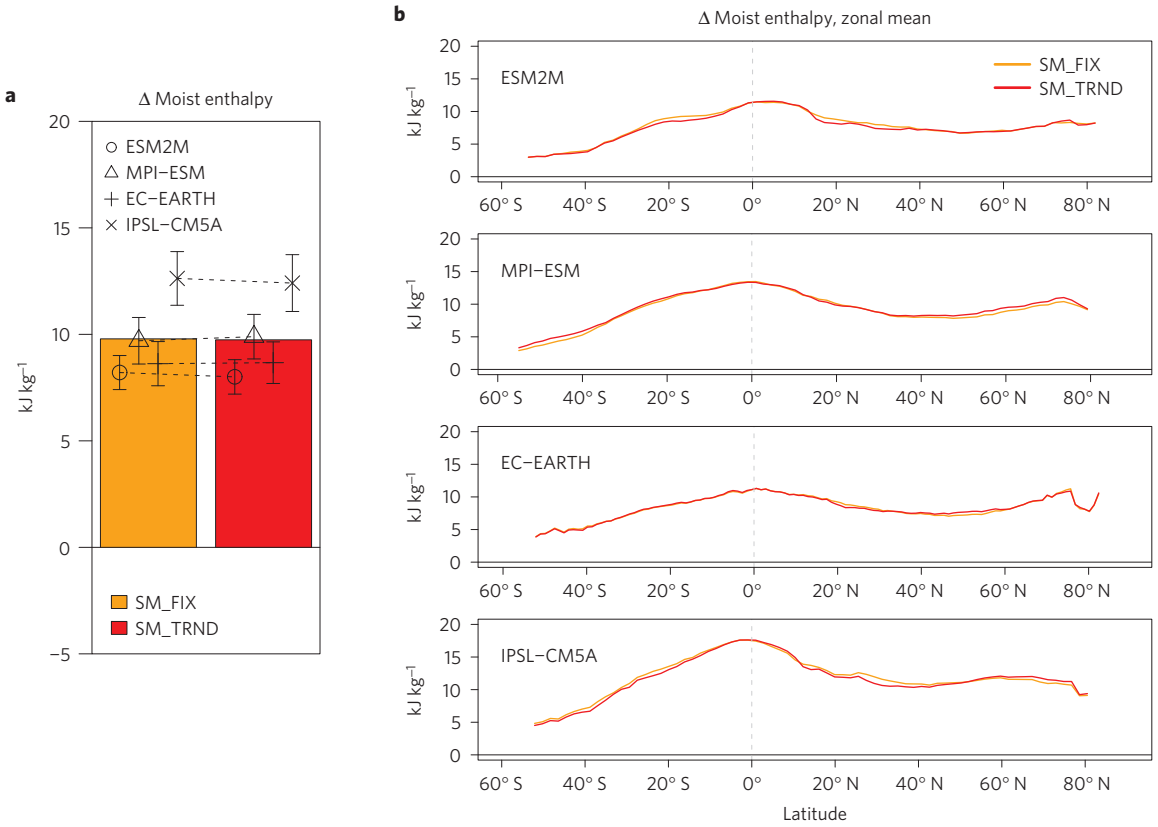

Figure 5 | Moist enthalpy changes over land. a, As Fig. 2, but for changes in moist enthalpy over land in SM_FIX and SM_TRND. **b**, Zonal change (future minus present) in moist enthalpy over land in the four models in SM_FIX and SM_TRND.

from reduced plant water requirements. It is also associated with increased $P - E$ over land (not shown). Thus, atmospheric aridity in that case may be decoupled from impacts on vegetation[30] and water resources[29,30]. Part of the diagnosed aridity increase in climate model projections[1–6] should thus be interpreted in this context[30].

Previous studies have argued that fundamental aspects of terrestrial climate change, such as contrasting land–ocean temperature and relative humidity changes, are constrained by oceanic warming and associated atmospheric processes[4,5,14,15,18–21]. Our results further highlight the essential contribution of amplifying land surface feedbacks. We interpret our findings in light of previously proposed ocean–atmosphere arguments by showing that, despite different changes in T and Q in SM_FIX and SM_TRND, the increase in moist enthalpy over land, which combines temperature and humidity changes (Methods), is similar in both simulations (Fig. 5). Recalling that, for each model, SSTs are identical in both simulations, this is consistent with projected zonally uniform changes in equivalent potential temperature over land and oceans[18], and highlights an important constraint on land climate change from oceanic warming. Interestingly, because physiological heat stress (for humans and other mammals) is closely related to moist enthalpy[18], this result also reinforces confidence in model projections of future heat stress over land, as changes are tightly coupled to ocean warming and not dependent on the less certain land hydrological response. Aridity changes, on the other hand, reflect the response of the coupled land–atmosphere system, and are affected by the land hydrological response, which partitions the enthalpy increase into T and Q changes—ultimately amplifying aridity. To improve projections of changes in terrestrial aridity and associated impacts, it will thus be necessary to better understand and constrain simulated land hydrology and associated land–atmosphere feedbacks in climate model projections.

Methods

Methods and any associated references are available in the online version of the paper.

Received 12 November 2015; accepted 12 April 2016; published online 16 May 2016

References

1. Cook, B. I., Smerdon, J. E., Seager, R. & Coats, S. Global warming and 21st century drying. *Clim. Dynam.* **43,** 2607–2627 (2014).
2. Feng, S. & Fu, Q. Expansion of global drylands under a warming climate. *Atmos. Chem. Phys.* **13,** 10081–10094 (2013).
3. Scheff, J. & Frierson, D. M. W. Terrestrial aridity and its response to greenhouse warming across CMIP5 climate models. *J. Clim.* **28,** 5583–5600 (2015).
4. Fu, Q. & Feng, S. Responses of terrestrial aridity to global warming. *J. Geophys. Res. Atmos.* **119,** 7863–7875 (2014).
5. Sherwood, S. & Fu, Q. A drier future? *Science* **343,** 737–739 (2014).
6. Lin, L., Gettelman, A., Feng, S. & Fu, Q. Simulated climatology and evolution of aridity in the 21st century. *J. Geophys. Res. Atmos.* **120,** 5795–5815 (2015).
7. Seneviratne, S. I. *et al*. Impact of soil moisture-climate feedbacks on CMIP5 projections: first results from the GLACE-CMIP5 experiment. *Geophys. Res. Lett.* **40,** 5212–5217 (2013).
8. Berg, A. *et al*. Interannual coupling between summertime surface temperature and precipitation over land: processes and implications for climate change. *J. Clim.* **28,** 1308–1328 (2015).
9. Lorenz, R. *et al*. Influence of land–atmosphere feedbacks on temperature extremes in the GLACE-CMIP5 ensemble. *J. Geophys. Res. Atmos.* **121,** 607–623 (2016).
10. Scheff, J. & Frierson, D. M. W. Scaling potential evapotranspiration with greenhouse warming. *J. Clim.* **27,** 1539–1558 (2014).
11. Pendergrass, A. G. & Hartmann, D. L. The atmospheric energy constraint on global-mean precipitation change. *J. Clim.* **27,** 757–768 (2014).
12. Manabe, S., Stouffer, R. J., Spelman, M. K. & Bryan, K. Transient responses of a coupled ocean-atmosphere model to gradual changes of atmospheric CO_2. Part I: Annual mean response. *J. Clim.* **4,** 785–818 (1991).

13. Sutton, R. T., Dong, B. W. & Gregory, J. M. Land/sea warming ratio in response to climate change: IPCC AR4 model results and comparison with observations. *Geophys. Res. Lett.* **34,** L02701 (2007).
14. Joshi, M. M., Gregory, J. M., Webb, M. J., Sexton, D. M. H. & Johns, T. C. Mechanisms for the land/sea warming contrast exhibited by simulations of climate change. *Clim. Dynam.* **30,** 455–465 (2008).
15. Fasullo, J. T. Robust land–ocean contrasts in energy and water cycle feedbacks. *J. Clim.* **23,** 4677–4693 (2010).
16. Simmons, A., Willett, K. M., Jones, P. D., Thorne, P. W. & Dee, D. Low-frequency variations in surface atmospheric humidity, temperature, and precipitation: inferences from reanalyses and monthly gridded observational data sets. *J. Geophys. Res.* **115,** D01110 (2010).
17. Laîné, A., Nakamura, H., Nishii, K. & Miyasaka, T. A diagnostic study of future evaporation changes projected in CMIP5 climate models. *Clim. Dynam.* **42,** 2745–2761 (2014).
18. Byrne, M. P. & O'Gorman, P. A. Link between land–ocean warming contrast and surface relative humidities in simulations with coupled climate models. *Geophys. Res. Lett.* **40,** 5223–5227 (2013).
19. Byrne, M. & O'Gorman, P. Land–ocean warming contrast over a wide range of climates: convective quasi-equilibrium theory and idealized simulations. *J. Clim.* **26,** 4000–4016 (2013).
20. Rowell, D. P. & Jones, R. G. Causes and uncertainty of future summer drying over Europe. *Clim. Dynam.* **27,** 281–299 (2006).
21. O'Gorman, P. A. & Muller, C. J. How closely do changes in surface and column water vapor follow Clausius–Clapeyron scaling in climate-change simulations? *Environ. Res. Lett.* **5,** 025207 (2010).
22. Cao, L. *et al*. Importance of carbon dioxide physiological forcing to future climate change. *Proc. Natl Acad. Sci USA* **107,** 9513–9518 (2010).
23. Collins, M. R. *et al*. in *Climate Change 2013: The Physical Science Basis* (eds Stocker, T. F. *et al*.) 1029–1136 (IPCC, Cambridge Univ. Press, 2013).
24. Koster, R. D. *et al*. On the nature of soil moisture in land surface models. *J. Clim.* **22,** 4322–4335 (2009).
25. Orlowsky, B. & Seneviratne, S. I. Elusive drought: uncertainty in observed trends and short- and long-term CMIP5 projections. *Hydrol. Earth Syst. Sci.* **17,** 1765–1781 (2013).
26. Koster, R. D. *et al*. Regions of strong coupling between soil moisture and precipitation. *Science* **305,** 1138–1140 (2004).
27. Spracklen, D. V. & Garcia-Carreras, L. The impact of Amazonian deforestation on Amazon basin rainfall. *Geophys. Res. Lett.* **42,** 9546–9552 (2015).
28. Sheffield, J., Wood, E. F. & Roderick, M. L. Little change in global drought over the past 60 years. *Nature* **491,** 435–438 (2012).
29. Greve, P. & Seneviratne, S. I. Assessment of future changes in water availability and aridity. *Geophys. Res. Lett.* **42,** 5493–5499 (2015).
30. Roderick, M. L., Greve, P. & Farquhar, G. D. On the assessment of aridity with changes in atmospheric CO_2. *Wat. Resour. Res.* **51,** 5450–5463 (2015).

Acknowledgements

The contribution of A.B. was supported by NSF Postdoctoral Fellowship AGS-1331375. We acknowledge the World Climate Research Programme's Working Group on Coupled Modelling, which is responsible for CMIP, and we thank the climate modelling groups for producing and making available their model output. For CMIP, the US Department of Energy's Program for Climate Model Diagnosis and Intercomparison provides coordinating support and led development of software infrastructure in partnership with the Global Organization for Earth System Science Portals. The authors thank T. Knutson and I. Held for providing comments on an earlier version of the manuscript.

Author contributions

A.B. designed the study, conducted the analysis and wrote the manuscript. K.F., B.L. and P.C.D.M. advised on the approach followed and the interpretation of results. All authors contributed to the manuscript preparation. S.I.S. and B.v.d.H. designed and led the GLACE-CMIP5 experiment. R.L., S.H., A.M., F.C., A.D. and S.M. performed model experiments in their respective groups.

Additional information

Supplementary information is available in the online version of the paper. Reprints and permissions information is available online at www.nature.com/reprints. Correspondence and requests for materials should be addressed to A.B.

Competing financial interests

The authors declare no competing financial interests.

Methods

Simulations. We use simulations from several models participating in the GLACE-CMIP5 experiment[7]. All simulations are land–atmosphere transient climate change simulations extending over 1950–2100, with transient sea surface temperatures (SSTs), sea ice and radiative forcing agent concentrations prescribed from the corresponding CMIP5 simulations (using the historical simulations over 1950–2005 and the representative concentration pathway 8.5 (RCP8.5) scenario thereafter). In simulation SM_FIX, for each model, total soil moisture was overridden throughout the simulation, pixel by pixel, by the climatological seasonal cycle of soil moisture over 1971–2000 from the corresponding historical, coupled CMIP5 simulation. Simulation SM_TRND is identical to SM_FIX except that a centred, 30-year moving average transient climatology of soil moisture (from the historical and then RCP8.5 coupled simulation) is used to prescribe soil moisture (in the first and last 15 years the climatology of 1950–1979 and 2071–2100, respectively, are used). Simulations SM_TRND and SM_FIX thus share similar boundary conditions throughout the simulations (SSTs, sea ice and radiative forcing agents), but simulation SM_TRND includes long-term changes in mean soil moisture, whereas SM_FIX does not. In both SM_FIX and SM_TRND, soil moisture was prescribed at every level in the soil column; depending on the model, soil moisture was prescribed either at every time step, or daily, or monthly with interpolation between the midpoints of the adjacent months for each time step.

Similarly, simulations NoFERT and CTL also share the same boundary conditions. However, in simulation NoFERT, atmospheric CO_2 concentrations seen by photosynthesis are kept constant through the twenty-first century to the 1971–2000 annual mean. In simulation CTL, CO_2 used for photosynthesis is identical to atmospheric CO_2 (in both runs soil moisture is fully interactive).

The reader is referred to refs 7 and 9 for further discussion of the models and the experimental protocol of GLACE-CMIP5. For simulations SM_FIX and SM_TRND, six models provided data. We use simulations from four models. Two models were discarded owing to identified issues with the simulations related to the soil moisture override technique. The models used are the Geophysical Fluid Dynamic Laboratory ESM2M model, the European Consortium Earth System Model (EC-EARTH), the Max Planck Institute for Meteorology Earth System Model (MPI-ESM), and the Institut Pierre-Simon Laplace Coupled Model, version 5A (IPSL-CM5A). Excluded from the comparison between SM_FIX and SM_TRND were the Australian Community Climate and Earth System Simulator (ACCESS) model ESM and the National Center for Atmospheric Research (NCAR) Community Climate System Model, version 4 (CCSM4). Even though excluded, results from these models were qualitatively similar to other models.

For simulations NoFERT and CTL, three models provided data: the ACCESS model, MPI-ESM and NCAR's CCSM4. Because of missing surface wind data in CCSM4, we used a fixed mean surface wind speed ($3.4\,m\,s^{-1}$, computed as the mean over land from ACCESS and MPI-ESM) to compute E_p and P/E_p for this model. Relative to changes in energy availability and vapour-pressure deficit, Penman–Monteith E_p is relatively insensitive to wind speed[1,10]. Results are thus not qualitatively affected by this approximation: a similar approximation for other models yielded results consistent with those presented here (Fig. 4).

In addition, because of issues with the consistency of SSTs between historical and future simulations in the ACCESS simulations, we define present day in ACCESS as 2007–2037, rather than 1971–2000. This does not significantly affect our conclusions, as results for other models are similar whichever way present is defined.

Only land-only pixels were considered when computing global and zonal averages over land (Figs 2–5); mixed sea–land pixels were excluded. Greenland and Antarctica were removed. Averages are computed on the models' native grids.

Calculation of evaporative demand. There are numerous ways to estimate the potential evaporation rate of the land surface under given climatic conditions. In this study we consider the evaporation that would occur from an open body of water subjected to similar climatic conditions. It is estimated from the Penman equation, in the form:

$$E_p = \frac{\Delta}{\Delta+\gamma}R_{net} + \frac{\gamma}{\Delta+\gamma}6.43(1+0.536U)D \quad (1)$$

where E_p is evaporative demand, R_{net} is surface net radiation, U is wind speed at 2 m, D is the vapour-pressure deficit, γ is the psychometric constant, and Δ is the slope of the saturated vapour pressure against air temperature. This form is equivalent to the Penman–Monteith evapotranspiration of a reference vegetation cover[10] when stomatal resistance is set to zero. Equation (1) is the recommended form of the Penman equation[28].

Note that surface wind speed is provided at 10 m in standard climate model outputs. We interpolate 10-m wind to two metres with a logarithmic approximation, assuming roughness parameters of open water.

We also calculate E_p simply as net radiation, as well as with the Priestley–Taylor formulation, which does not consider vapour-pressure deficits:

$$E_p = \alpha\frac{\Delta(R_{net}-G)}{(\Delta+\gamma)} \quad (2)$$

where G is the heat flux into the ground, $R_{net}-G$ is approximated here as the sum of the latent and sensible heat fluxes, and we use 1.26 for scaling factor α.

Finally, we also compute E_p as potential evapotranspiration (PET) using the Penman–Monteith evapotranspiration of a virtual, well-watered reference crop with known physical characteristics, as done in ref. 10, using:

$$\mathrm{PET} = \left[\frac{\Delta(R_{net}-G)+\rho_a c_p e^*(T_a)(1-\mathrm{RH})C_H U}{\Delta+\gamma(1+r_s C_H U)}\right] \Big/ L_v \quad (3)$$

where $e^*(T_a)$ is the saturation vapour pressure at a given temperature T, RH is the relative humidity, U is surface wind speed, C_H is a scalar transfer coefficient (which depends on prescribed surface roughness parameters associated with the reference crop), r_s is the (prescribed) bulk stomatal resistance under well-watered conditions ($r_s = 70\,sm^{-1}$), ρ_a is the air density, c_p is the air specific heat, L_v is the latent heat of phase change of vaporization. The reader is referred to ref. 10 for further details.

Decomposition of P/E_p change. According to error propagation rules, the fractional change in $\mathrm{AI} = P/E_p$ can be decomposed as follows:

$$\frac{\Delta(P/E_p)}{P/E_p} \sim \frac{\Delta P}{P} - \frac{\Delta E_p}{E_p}$$

where Δ refers to the future-minus-present change and the values in the denominator are present-day means. Thus, the change in P/E_p can be approximated by a precipitation-change-induced term:

$$\frac{P}{E_p}\frac{\Delta P}{P}$$

and an E_p-change-induced term:

$$\frac{P}{E_p}\frac{\Delta E_p}{E_p}$$

Calculation of moist enthalpy. Moist enthalpy, H, is defined as $C_pT + L_vq$, where C_p is the heat capacity of air at constant pressure, T is air temperature, L_v is the latent heat of phase change of water vapour, and q is the specific humidity of air. It characterizes the energy content of a parcel of air from both temperature and humidity. Here we use the classic approximation for $C_pT = (1.007T - 0.026)$ and $L_v = (2,502 - 0.538T)$ (https://pielkeclimatesci.wordpress.com/2010/07/22/guest-post-calculating-moist-enthalpy-from-usual-meteorological-measurements-by-francis-massen).